GEOPHYSICS, VOL. 69, NO. 2 (MARCH-APRIL 2004); P. 583–591, 7 FIGS.
10.1190/1.1707078

Finite-difference modeling of viscoelastic and anisotropic wave propagation using the rotated staggered grid

Erik H. Saenger* and Thomas Bohlen‡

ABSTRACT

We describe the application of the rotated staggered-grid (RSG) finite-difference technique to the wave equations for anisotropic and viscoelastic media. The RSG uses rotated finite-difference operators, leading to a distribution of modeling parameters in an elementary cell where all components of one physical property are located only at one single position. This can be advantageous for modeling wave propagation in anisotropic media or complex media, including high-contrast discontinuities, because no averaging of elastic moduli is needed. The RSG can be applied both to displacement-stress and to velocity-stress finite-difference (FD) schemes, whereby the latter are commonly used to model viscoelastic wave propagation. With a von Neumann-style anlysis, we estimate the dispersion error of the RSG scheme in general anisotropic media. In three different simulation examples, all based on previously published problems, we demonstrate the application and the accuracy of the proposed numerical approach.

INTRODUCTION

Numerical modeling of seismic wave propagation in realistic media is an important tool in earthquake and exploration seismology. It has been used to support interpretations of field data, to provide synthetic data for testing processing techniques and acquisition parameters, and to improve seismologists' understanding of seismic wave propagation. A general overview of different techniques and applications can be found in Carcione et al. (2002) and references therein. Since the widely used finite-difference (FD) approaches are based on the wave equation without physical approximations, the methods account not only for direct waves, primary reflected waves, and multiply reflected waves, but also for surface waves, head waves, converted reflected waves, and waves observed in ray-theoretical shadow zones (Kelly et al., 1976).

Staggered-grid FD operators are commonly applied to compute the derivatives in the wave equations for elastic, viscoelastic, and anisotropic media (e.g., Virieux, 1986; Levander, 1988; Robertsson et al., 1994; Igel et al., 1995). However, the standard staggered FD grid [according to Virieux (1986)] can become unstable when the medium exhibits high contrasts in material properties. Boundary conditions of the elastic wavefield at a free surface, i.e., the high-contrast discontinuity between vacuum and rock, must be defined in the FD algorithm (e.g., Robertsson, 1996; Graves, 1996; Hestholm and Ruud, 1998; Oprsal and Zahradnik, 1999). By using the so-called rotated staggered-grid (RSG) technique (Saenger et al., 2000), high-contrast discontinuities can be incorporated without applying explicit boundary conditions and without averaging elastic moduli. For this reason, the rotated staggered grid is a powerful rock physics tool for studying effective velocities in dry and saturated fractured media (Saenger and Shapiro, 2002; Saenger et al., 2002; Saenger et al., 2003). Additionally, the RSG has been applied to study scattering attenuation in random media (Müller and Shapiro, 2001; Müller et al., 2002) and for modeling seismic waves around a tunnel with irregular walls (Bohlen et al., 2003).

The RSG has so far been applied to displacement-stress formulations of the elastic-wave equation for isotropic media (Saenger et al., 2000). Our first objective is to show that the RSG technique can also be adopted to a velocity-stress formulation of the wave equation. Velocity-stress formulations are commonly used to model seismic wave absorption (Carcione et al., 1988; Robertsson et al., 1994; Bohlen, 2002). By applying the RSG to the 3D viscoelastic wave equation, it becomes possible to simulate the propagation of seismic waves in a viscoelastic medium containing voids or free surface topography without applying explicit boundary conditions at the high-contrast interfaces. In our first modeling example, we use the new velocity-stress RSG algorithm to simulate seismic waves in an elastic and viscoelastic model with 3D topography of

Published on Geophysics Online November 25, 2003. Manuscript received by the Editor December 17, 2002; revised manuscript received November 17, 2003.
*Freie Universität Berlin, Fachrichtung Geophysik, Building D, Malteserstrasse 74-100, 12249 Berlin, Germany. E-mail: saenger@geophysik.fu-berlin.de.
‡Universität Kiel, Institut für Geowissenschaften, Abteilung Geophysik, Otto-Hahn-Platz 1, 24118 Kiel, Germany. E-mail: tbohlen@geophysik.uni-kiel.de.

the free surface. We compare our seismograms with previously published modeling results of Ohminato and Chouet (1997) and find good agreement.

The second objective of this paper is the application of the RSG technique to the elastic-wave equation for anisotropic media. Many papers (e.g., Komatitsch et al., 2000; Carcione et al., 2002) report a disadvantage in using standard staggered grids for anisotropic media with symmetry lower than orthorhombic. Standard staggering implies that off-diagonal stress and strain components are not defined at the same location (Igel et al., 1995). When evaluating the stress–strain relation, it is necessary to sum over a linear combination of the elastic constants multiplied by the strain components. Hence, some terms of the stress components must be interpolated to obtain values at the locations where the diagonal components are defined. This fact leads to an additional error in the dispersion analysis (Igel et al., 1995) and is computationally intricate (i.e., CPU intensive). For the rotated staggered grid such an interpolation is not necessary. By analyzing the numerical dispersion, we show that the RSG can be advantageous for modeling general anisotropic media. The modeling of elastic waves in an anisotropic medium using the RSG is demonstrated using two examples.

APPLICATION OF THE ROTATED STAGGERED GRID TO THE WAVE EQUATIONS FOR ANISOTROPIC AND VISCOELASTIC MEDIA

The basic numerical procedures for velocity-stress and displacement-stress FD schemes for elastic media are well known (e.g., Virieux, 1986; Luo and Schuster, 1990). Viscoelasticity can be implemented in time-domain velocity-stress schemes in a very efficient way (Robertsson et al., 1994). The formulation of the viscoelastic wave equation is based on a rheological rock model called generalized standard linear solid. For this model the attenuation parameters—namely, the stress relaxation times $\tau_{\sigma l}$ [for each relaxation mechanism (l)] and the τ-parameter—have to be optimized for the desired frequency-independent Q-factor (Blanch et al., 1995; Bohlen, 2002).

The differential equations for the velocity-stress and the displacement-stress FD scheme were recast into discretized equivalents using staggered-grid approaches. As a result, all modeling parameters are distributed at different (staggered and nonstaggered) positions within the FD grid. For the sake of simplicity, we first consider an isotropic elastic medium in two dimensions with equal grid spacing in the **x**- and **z**-directions. However, the distribution of modeling parameters within the 2D finite-difference cells shown in Figure 1 have also been transfered to rectangular cells in three dimensions.

In Figures 1a and 1c, we show the distribution of modeling parameters using standard staggered FD operators for the velocity-stress and the displacement-stress schemes, respectively. To place all components of one physical property (e.g., stress, strain, or elastic constants) only at one single location for the RSG schemes, we change the directions of the derivatives from the axis to the room diagonals (Figures 1b and 1d). The necessary FD operators for the rotated and the standard staggered grid are discussed in detail in Saenger et al. (2000).

As described in Saenger and Shapiro (2002), the density defined at the corners of the FD cell has to be averaged by the density values of the surrounding cells. This procedure is in principle equivalent to the heterogeneous approaches described in Graves (1996) and Moczo et al. (2002). The main difference is that it is unnecessary to average any elastic constants because, for the rotated staggered grid, they are all placed in the center of the FD cell. As a consequence, the plane going through the staggered position of the densities (i.e., in between the position of the elastic constants) is the location of the material discontinuity between two different media. The consideration performed in Moczo et al. (2002) shows that the arithmetic averaging of densities described above leads to continuity of displacement and traction at the interface.

To realize a free surface (the highest possible heterogeneity), we simply set the elastic constants above the surface to zero ($c_{ijkl} = 0$) and the density close to zero (to avoid division by zero), which approximates a vacuum. It is not necessary to define any additional boundary conditions. This procedure is comparable with vacuum formalisms (Boore, 1970; Zahradink and Hron, 1992; Graves, 1996). The numerical accuracy of the RSG for modeling SH-wave scattering at empty fractures (also a realization of the highest possible heterogeneity) was successfully verified by comparison with an analytical solution (Krüger et al., 2002). Bohlen and Saenger (2003) tested the accuracy of the 3D viscoelastic RSG algorithm for Lamb's problem. When modeling Rayleigh waves propagating along a planar free surface aligned with the grid, a high level of accuracy was obtained if more than 30 gridpoints per minimum wavelength were used and second-order spatial FD operators were applied at the free surface. Near a free surface, the application of high-order FD operators is generally not useful because of the strong fluctuation of the wavefield at this boundary. Furthermore, for modeling fractured media (e.g., Saenger and Shapiro, 2002), the application of high-order operators when the length of the operator exceeds the dimension of a thin crack will obviously produce wrong results.

In the viscoelastic case of the velocity-stress scheme (Figure 1b), the attenuation parameters $\tau_{\sigma l}$ and τ have the same position as the components of the stress tensor σ_{ij}. For the rotated staggered grid, in the case of anisotropic elastic media, all elements of the elastic stiffness tensor c_{ij} have the same position as the elastic material parameters in the isotropic case (Lamé parameters λ and μ; see Figures 1b and 1d). This distribution of elastic parameters for the RSG is advantageous for modeling in general anisotropic media because no interpolation operator (Igel et al., 1995) is necessary to calculate the Hooke summation in the modeling algorithm.

NUMERICAL STABILITY AND DISPERSION

Saenger et al. (2000) investigate the numerical stability and grid dispersion of the RSG for isotropic elastic media. Though only the displacement-stress scheme is explicitly treated in this paper, all results apply to the velocity-stress scheme as well [for details, refer to Marfurt (1984), Sei (1995), and Moczo et al. (2000)].

We extend the dispersion relation found by Igel et al. (1995) for general anisotropic 3D media using a $O(\Delta t^{N_{time}}, \Delta x^{N_{space}})$ standard staggered grid to the rotated staggered grid. The dispersion relation is valid for displacement-stress and velocity-stress FD schemes. The extension of the elastic dispersion analysis, described below, to the viscoelastic case is analogous to Robertsson et al. (1994).

The general dispersion equation valid for the RSG and the standard staggered-grid FD scheme expresses the frequency $\tilde{\omega}$ as a function of the numerical wavenumber $\tilde{\mathbf{k}}$, the eigenvalues $\lambda_l(\tilde{\mathbf{k}}, c_{IJ}, \rho, d_{\overrightarrow{ij}}, d_{\overleftarrow{ji}})$ [$l = 1, 2, 3$ for qP-, qS1-, and qS2-waves] of the matrix $\hat{\mathbf{M}}$, and the order of the time extrapolation N_{time} as

$$\tilde{\omega}_l(\mathbf{k}, \Delta t) = \frac{2}{\Delta t} \arcsin \times \sqrt{-\frac{1}{2} \sum_{n=1}^{N_{time}/2} (-1)^n \lambda_l^n \left(\tilde{\mathbf{k}}, c_{IJ}, \rho, d_{\overrightarrow{ij}}, d_{\overleftarrow{ji}}\right) \frac{\Delta t^{2n}}{(2n)!}} \quad (1)$$

[similar to equation (45) of Igel et al. (1995); they use another definition of the time extrapolation and there is a printing error: $\lambda_i^{2n}(\mathbf{k})$ must be replaced by $\lambda_i^n(\mathbf{k})$], where Δt is the time increment of the FD scheme used, c_{IJ} are the elements of the elastic stiffness tensor, ρ denotes the density, and $d_{\overrightarrow{ij}}, d_{\overleftarrow{ji}}$ are interpolation operators. The definition of $\hat{\mathbf{M}}$ is given in equation (A-7) of the Appendix.

For the standard staggered grid, the following numerical wavenumber $\tilde{k}_j$ and the interpolation operators $d_{\overrightarrow{ij}}$ and $d_{\overleftarrow{ji}}$ must be used:

$$\tilde{k}_j = \frac{2}{\Delta x_j} \sum_{m=1}^{N_{space}/2} \left[p_m \sin\left(k_j \frac{2m-1}{2} \Delta x_j \right) \right], \quad (2)$$

where N_{space} is the order of space extrapolation [equation (5) of Crase (1990) and equation (35) of Igel et al. (1995)], and

$$d_{\overrightarrow{ij}} = d_{\overleftarrow{ji}} = 2 \sum_{m=1}^{N_{space}/2} \left[d_m \cos\left(k_i \frac{2m-1}{2} \Delta x_i \right) \times \cos\left(k_j \frac{2m-1}{2} \Delta x_j \right) \right] \quad (3)$$

[equation (22) and associated text of Igel et al. (1995)], where Δx_j is the grid spacing in the j-direction, k_j is the jth component of the wavenumber $\mathbf{k}$, p_m are the finite-difference coefficients (e.g., Holberg, 1987; Igel et al., 1995; Karrenbach, 1995), and d_m are the coefficients of the interpolation operator.

For the rotated staggered grid, $\tilde{k}_j$ in equation (1) must be substituted by the numerical wavenumber $\tilde{k}_j^{rot}$. The interpolation operators $d_{\overrightarrow{ij}}^{rot}$ and $d_{\overleftarrow{ji}}^{rot}$ are equal to one since this kind of interpolation is not necessary for the RSG, i.e.,

$$\tilde{k}_j^{rot} = \frac{2}{\Delta x_j} \sum_{m=1}^{N_{space}/2} \left[p_m \sin\left(k_j \frac{2m-1}{2} \Delta x_j \right) \times \prod_{\substack{i=1 \\ i \neq j}}^{3} \cos\left(k_i \frac{2m-1}{2} \Delta x_i \right) \right] \quad (4)$$

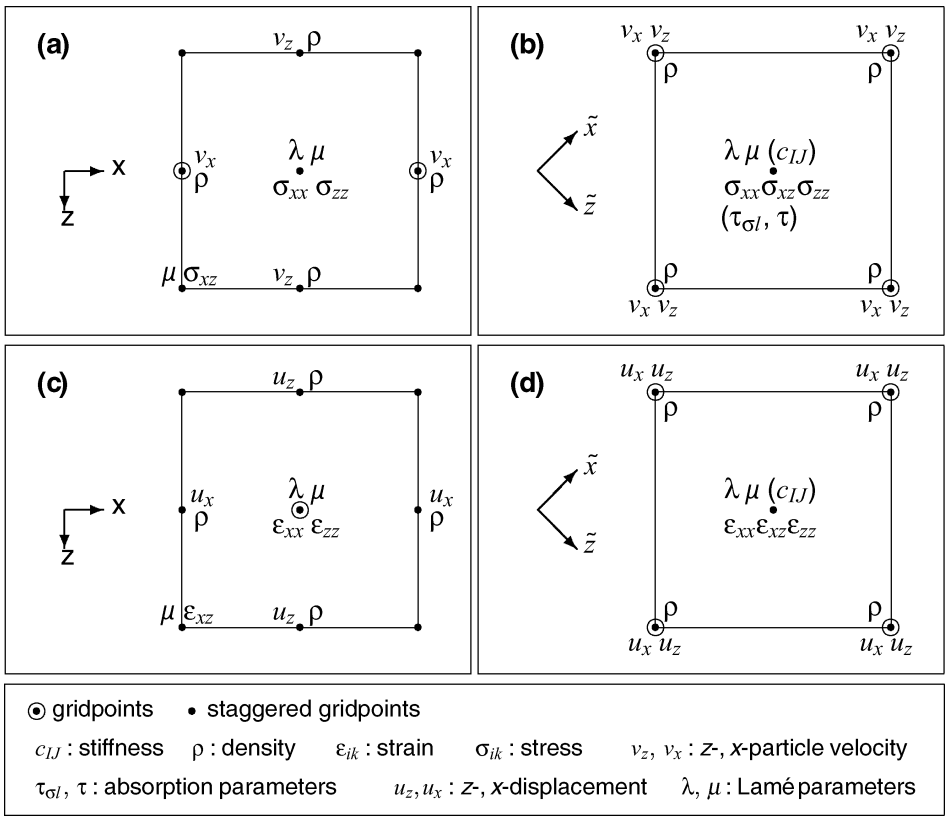

Figure 1. Elementary cells of different staggered grids. Locations where strains, displacements, velocities, and elastic parameters are defined. (a) Velocity-stress FD technique using a standard staggered grid (e.g., Virieux, 1986). (b) Velocity-stress FD technique using the rotated staggered grid. (c) Displacement-stress FD technique using a standard staggered grid (e.g., Karrenbach, 1995). (d) Displacement-stress FD technique using the rotated staggered grid. For the RSG all components of one physical property are placed only at one location [(b) and (d)].

[derivation according to Crase (1990)] and

$$d_{\overrightarrow{ij}}^{rot} = d_{\overleftarrow{ji}}^{rot} = 1. \quad (5)$$

The stability criterion for an $O(\Delta t^{N_{time}}, \Delta x^{N_{space}})$ FD scheme can be found by analyzing the following inequality (Crase, 1990):

$$0 \le -\frac{1}{2} \sum_{n=1}^{N_{time}/2} (-1)^n \lambda_l^n \left(\tilde{\mathbf{k}}, c_{IJ}, \rho, d_{\overrightarrow{ij}}, d_{\overleftarrow{ji}}\right) \frac{\Delta t^{2n}}{(2n)!} \le 1. \quad (6)$$

For a general anisotropic medium this is not easily evaluated. However, the stability criterion for velocity-stress and displacement-stress RSG schemes (second-order time, i.e., $N_{time} = 2$) for isotropic media and equal grid spacing ($\Delta h = \Delta x_1 = \Delta x_2 = \Delta x_3$) can be found in Saenger et al. (2000):

$$\frac{\Delta t\, v_p}{\Delta h} \le \frac{1}{\left(\sum_{m=1}^{N_{space}/2} |p_m|\right)}. \quad (7)$$

In this equation, v_p denotes the compressional-wave velocity. Stability is increased for the 3D case by a factor of $\sqrt{3}$ compared to the standard staggered grid (Saenger et al., 2000). In the anisotropic case, a good approximation can be made by replacing v_p in equation (7) by the maximum phase velocity of the anisotropic medium (Igel et al. 1995).

For a comparison of both finite-difference schemes (i.e., the RSG and the standard staggered grid), we consider exactly the same triclinic medium as defined in equation (47) of Igel et al. (1995) [see also equation (A-8) in the Appendix]. We focus on the qS2-wave case where one can observe the maximum relative error of the phase velocity [see, e.g., Figure 6 of Igel et al. (1995)]. Here, we compare both schemes with a relative accuracy of $O(\Delta t^2, \Delta x^2)$ at 20% Nyquist frequency (dispersion parameter $H = |\mathbf{k}|\Delta h/(2\pi) = 0.1$) with $\Delta t = 0.146 \times 10^{-3}$ (s/m) Δx. This is about 75% of the stability limit for the standard staggered grid [see equation (46) of Igel et al. (1995)]. The coefficients of the FD operators and the interpolation operators used are $p_1 = 1$ and $d_1 = 0.5$, respectively. The results in Figure 2 can be qualitatively compared with the qS2-case shown in Figure 7 of Igel et al. (1995).

The conclusion of our dispersion analysis for the two different FD schemes is as follows: For this specific triclinic medium, the application of the rotated staggered grid is advantageous. In contrast to the standard staggered grid, the RSG has a lower maximum relative error (approximately 35%) and shows only a weak directional variation of the numerical dispersion error (i.e., the recommendation for spatial sampling is thus approximately 35% less restrictive than the standard staggered grid). However, for any other anisotropic medium one has to repeat the analysis described above for two reasons. First, the dispersion error in the general anisotropic case for staggered finite-difference grids depends on the length of the operators used, the symmetry system of the anisotropic medium, the orientation of the symmetry axis with respect to the coordinate axis, and the degree of anisotropy (Igel et al., 1995). For isotropic media, the standard staggered grid has a lower dispersion error than the rotated staggered grid (2D, factor $\sqrt{2}$; 3D, approximate factor $\sqrt{3}$). At the same time, the rotated staggered grid allows the calculation to be made with larger time steps [with the same corresponding factor; refer to Saenger et al. (2000) for a detailed discussion]. Second, for general anisotropic media, the ratio of the maximum relative error of the phase velocity between the RSG and the standard staggered grid depends on the dispersion parameter $H = |\mathbf{k}|\Delta h/(2\pi)$.

One result of the dispersion analysis described above that is not obvious is that the highest possible frequency (for two dimensions, a checkerboard-patterned wavefield) in the grid has a propagation velocity of zero. This frequency can be induced by a source implemented only at one single gridpoint or by very small-scale structures (a few gridpoints) within the FD grid. However, this visible high-frequency error can be removed after the simulation by arithmetic averaging of particle velocities or displacement components in the space domain.

VISCOELASTIC MODELING EXAMPLE

We apply the new viscoelastic velocity-stress RSG FD algorithm to simulate seismic wave propagation in a Gaussian hill. The same model has been studied by Ohminato and Chouet (1997). The objectives of this example are (1) to illustrate the capability of the algorithm to model free surface topography of a viscoelastic medium without applying explicit boundary conditions and (2) to evaluate the accuracy of the algorithm in the presence of surface topography by direct comparison with the numerical results published by Ohminato and Chouet (1997).

The surface topography is defined by the Gaussian function $z = a\exp(-r^2/a^2)$ with $r = \sqrt{x^2 + y^2}$ and $a = 1$ km. The seismic source is an explosive point source located 100 m below the surface of the hill at (−800 m, 0 m, 600 m) relative to the summit (Figure 3). The source wavelet is a Ricker signal with a center frequency of 1.5 Hz. The six receivers are located on the free surface. Their locations are indicated by triangles in Figure 3.

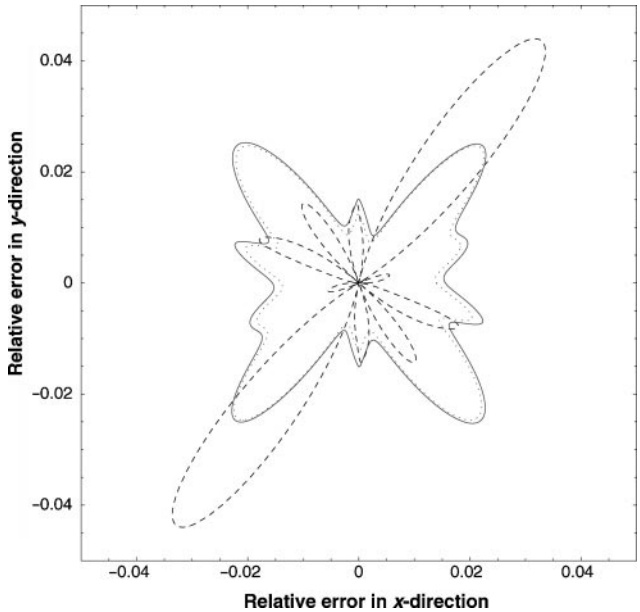

Figure 2. A comparison of the relative error of the phase velocity ($A_{rel} = |\omega(\mathbf{k})/(v_{ph}(\mathbf{k})|\mathbf{k}|) - 1|$) of the qS2-wave in the xz-plane between the standard staggered grid (dashed line) and the rotated staggered grid (solid line) with exactly the same modeling parameters. The medium has triclinic symmetry [equation (A-8)]. The dotted line is obtained for the rotated staggered grid with a time step increased by a factor of $\sqrt{3}$.

The P-velocity, S-velocity, and density of the hill are 3 km/s, 1.5 km/s, and 1200 kg/m^3, respectively. Above the hill surface, we set velocities to zero and density close to zero to simulate a vacuum.

Figure 3 shows the wavefield in the hill after 1.9 s. The shallow explosive source (black star in Figure 3) generates a strong Rayleigh wave that dominates the wavefield. The Rayleigh wave is best visible in the curl of the seismic wavefield (Figure 3, top). The hill increases the amplitude of the Rayleigh wave on the slope opposite to the source. This amplification is generated by energy focusing (scattering) at the summit of the hill. It cannot be observed for Rayleigh waves that do not pass the summit. Seismograms of displacement recorded at the six receiver locations are shown in Figure 4. The most prominent event in the seismograms is the Rayleigh wave. Because of the scattering of the Rayleigh wave at the hill, the horizontal components (u, v) show a strong waveform change with offset.

To explore which spatial sampling (Δh) is required to accurately simulate the Rayleigh-wave scattering at the hill, we compare modeling results with $\Delta h = 10$ m, 30 m, and 40 m in Figure 3. The grid intervals correspond to 50, 25, and 12 gridpoints per minimum wavelength, respectively. Second-order FD operators are used in the simulations. The model volume is divided into subdomains, each computed by a different CPU (Bohlen, 2002). The size of the total computational grid is $640 \times 400 \times 600$ gridpoints for $\Delta h = 10$ m and $180 \times 100 \times 180$ grid points for $\Delta h = 40$ m. The corresponding run times are 8 hours on 320 CPUs and 3 min on 320 CPUs, respectively. The comparison reveals that 25 gridpoints per minimum wavelength are sufficient to accurately simulate the Rayleigh-wave scattering at the hill. For modeling Rayleigh waves over larger distances, however, a finer grid spacing may be necessary (Xu et al., 1999; Bohlen and Saenger, 2003).

The RSG seismograms obtained with more than 25 gridpoints per minimum wavelength show quite good agreement

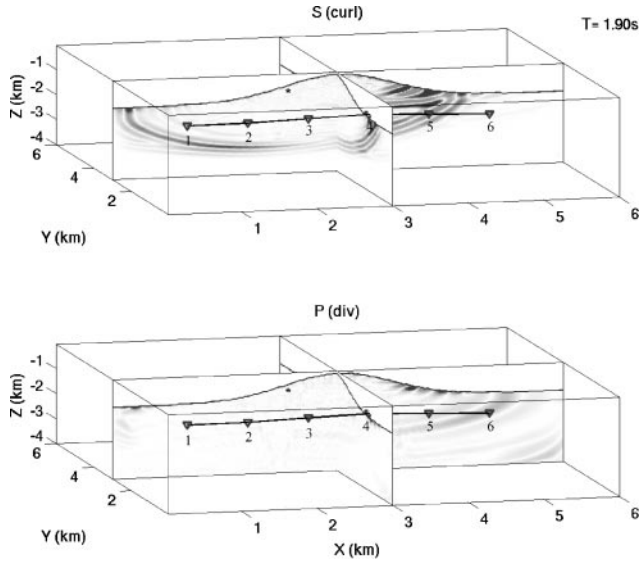

Figure 3. Snapshots of the curl (top) and divergence (bottom) of the wavefield in the Gaussian hill model. The location of the isotropic explosive point source is indicated by a black star. Receiver locations are denoted by triangles. The wavefield is dominated by a Rayleigh wave which is propagating along the surface of the hill. Note the scattering of the Rayleigh wave at the hill.

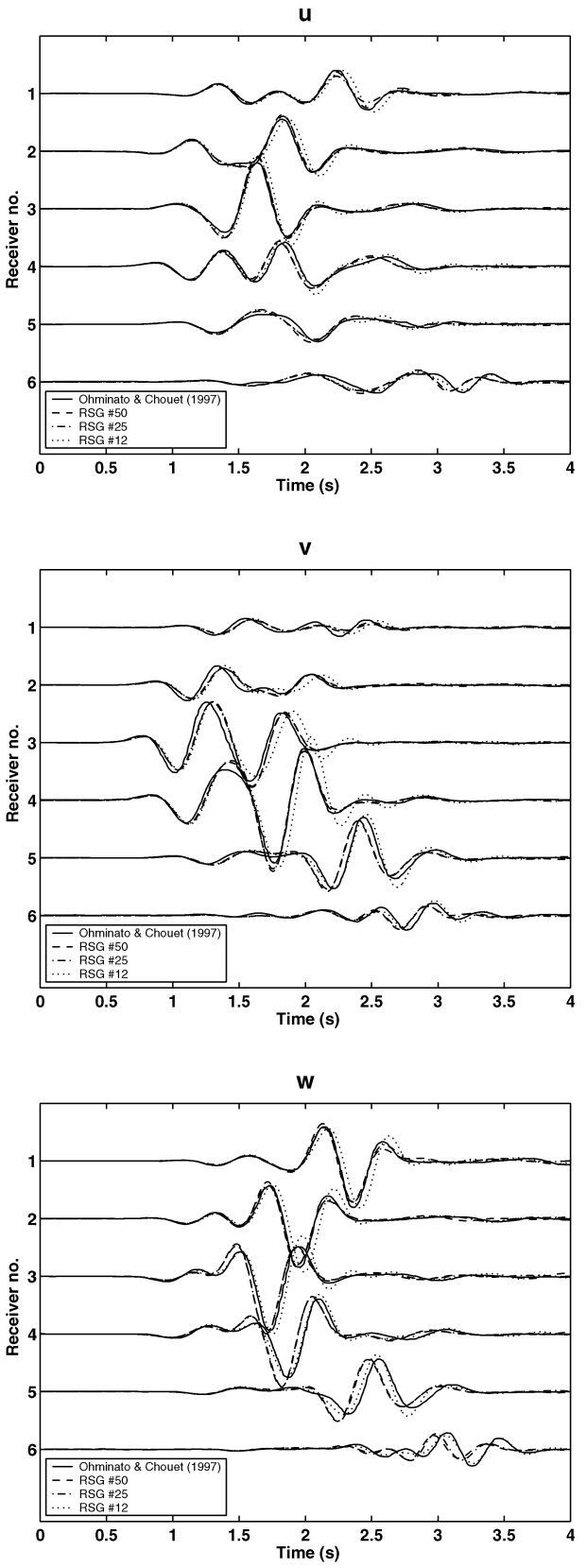

Figure 4. Seismograms of displacement recorded at the receiver locations indicated by triangles in Figure 3. The x-, y-, and z-components are denoted by u, v, and w, respectively. Seismograms computed using the RSG with 50, 25, and 12 gridpoints per minimum wavelength are compared with seismograms published by Ohminato and Chouet (1997).

with the modeling results obtained by Ohminato and Chouet (1997) (Figure 4). The latter seismograms have been digitized from Figure 18 of their paper to facilitate a direct comparison. Ohminato and Chouet (1997) also apply a finite-difference modeling technique but use a different approach to incorporate the free surface. In their approach the shear stresses are distributed on the 12 edges of the FD cell so that only shear stresses remain embedded within the solid region. With their method, 25 gridpoints per minimum wavelength are required for stable calculation. For the Gaussian hill model they use this value. Figure 4 reveals a good fit between the two different FD techniques for both arrival times and waveforms. This suggests that in this case both methods work well.

In a second example, we apply our new viscoelastic RSG algorithm to study the effect of seismic wave absorption in the hill. One relaxation mechanism is used in the simulation. The quality factor Q for both P- and S-waves lies between 20 and 35 for frequencies above 0.5 Hz, as shown in Figure 5b. The phase velocity dispersion resulting from absorption is approximately 2%. In Figure 5a, seismograms of vertical displacement for the elastic (solid line) and viscoelastic case (dashed line) are compared. Because of attenuation, amplitudes decrease significantly with offset. Slight waveform deviations can also be observed.

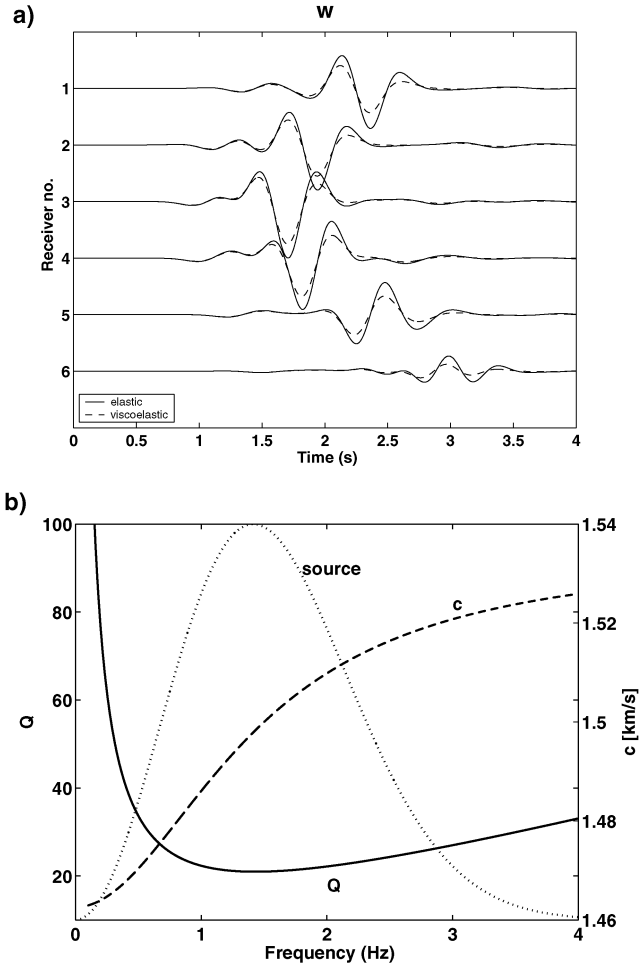

Figure 5. (a) Seismograms of vertical displacement for the elastic (solid) and viscoelastic (dashed) cases. (b) Quality factor (solid) and shear-wave velocity dispersion (dashed) in the frequency band of the source signal (dotted) used in the viscoelastic simulation. The absorption peak corresponds to a standard linear solid (one relaxation mechanism) with a relaxation frequency $[1/(2\pi\tau_\sigma)]$ of 1.5 Hz and $\tau = 0.1$.

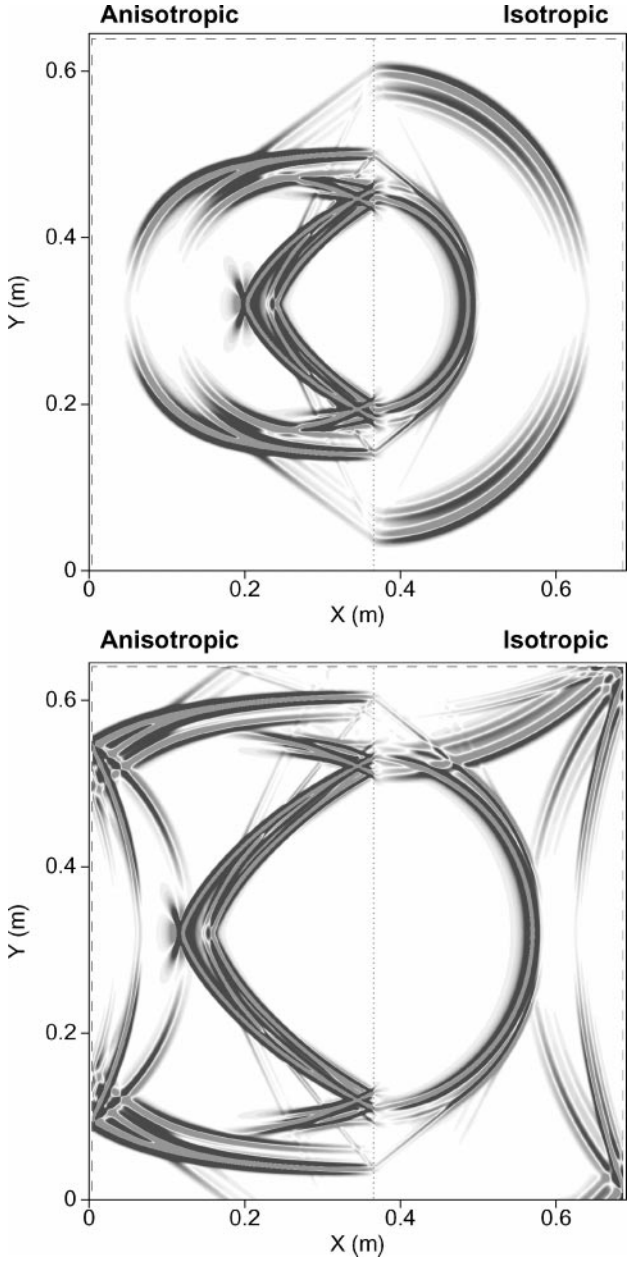

Figure 6. Two snapshots (y-displacement) at two different time steps of an anisotropic FD experiment using the rotated staggered grid. The model is composed of two media: a transversely isotropic zinc crystal with vertical symmetry axis on the left and an isotropic material on the right. The two media are surrounded on three sides by a thin vacuum layer. The solid-vacuum and the isotropic-anisotropic interface are marked with a dashed and a dotted line, respectively. A similar problem is studied Carcione et al. (1992) and Komatitsch et al. (2000).

ANISOTROPIC MODELING EXAMPLES

The RSG has also been applied to a displacement-stress formulation of the 2D and 3D elastic-wave equation for anisotropic media. In the first example, we demonstrate that the RSG allows for modeling anisotropic wave propagation in media with a strong contrast in elastic parameters. We built a 2D model with two different crystals. The two media have a total size of 0.68 m × 0.64 m. An equal grid spacing of $\Delta h = 0.5 \times 10^{-3}$ m is used. The left-hand side of the model is a transversely isotropic zinc crystal characterized by $c_{11} = 16.5 \times 10^{10}$ N/m^2, $c_{13} = 5 \times 10^{10}$ N/m^2, $c_{33} = 6.2 \times 10^{10}$ N/m^2, and $c_{55} = 3.96 \times 10^{10}$ N/m^2 and a density of $\rho = 7100$ kg/m^3. The medium on the right-hand side is an isotropic version of zinc with $c_{11} = 16.5 \times 10^{10}$ N/m^2, $c_{55} = 3.96 \times 10^{10}$ N/m^2, and $\rho = 7100$ kg/m^3. At the top, left, and right edges of the model, we introduce thin (5×10^{-3} m) vacuum layers ($c_{IJ} = 0$, $\rho = 0.00001$ kg/m^3). At the bottom edge, an absorbing boundary condition is applied. At the three free surfaces of the model, we use second-order FD operators. The FD order is gradually increased toward the interior of the model via four and six, up to eight [similar to Hestholm (2002)]. The source is a vertical point force located 20×10^{-3} m to the left of the interface in the anisotropic medium. The source–time function is a Ricker wavelet with dominant frequency $f_0 = 170$ kHz. The simulation uses 4000 time steps with an increment of $\Delta t = 25$ ns.

For the interpretation of the different phases in the first snapshot shown in Figure 6, we refer to Carcione et al. (1992) and Komatitsch et al. (2000). They have studied the same model but without considering the vacuum zones. In the second snapshot of the simulation (Figure 6), the reflections of the different waves at the three free surfaces are shown. This simulation is performed without applying explicit boundary conditions at the solid–vacuum interface.

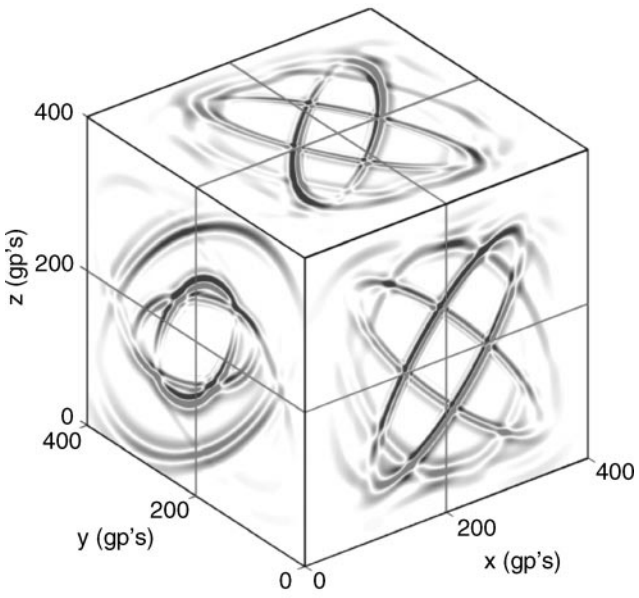

Figure 7. A snapshot (z-displacement) after 720 time steps (0.63s) of a large-scale 3D triclinic FD simulation using the rotated staggered grid. The model is a homogeneous block with an edge length of 2400 m [400^3 gridpoints (gp's)]. All three types of waves (qP, qS1, and qS2) can be identified. The elastic constants are given in equation (A-8).

For the second anisotropic example (Figure 7), we build a large-scale (400^3 gridpoints), homogeneous triclinic medium with an equal grid spacing of $\Delta h = 6$ m. The elastic constants are given in equation (A-8). An explosion source is placed in the center of the model. The dominant frequency of the Ricker wavelet is $f_{dom} = 6$ Hz with $\Delta t = 0.000876$ s. We estimate a maximum frequency of $f_{max} \approx 17$ Hz, which belongs to a dispersion parameter of $H = 0.1$. Therefore, using an $O(2,2)$ RSG FD scheme, the dispersion error displayed in Figure 2 corresponds directly to our modeling example. The computing time for 720 time steps is about 2 hours on 251 nodes of a Cray T3E computer. Because of the interpolation necessary to calculate the Hooke sum, using a standard staggered grid for this example is computationally expensive and less accurate (see Figure 2).

CONCLUSIONS

We have shown that the rotated staggered grid can be applied to the velocity–stress formulation of the viscoelastic-wave equation and to the displacement–stress formulation of the elastic-wave equation for anisotropic media. With a classical von Neumann-style accuracy analysis for the rotated staggered grid, we can estimate the dispersion error for any kind of anisotropic medium. Our examples show that the new algorithms allow for flexible modeling of seismic waves in complex viscoelastic and anisotropic media with strong-contrast interfaces of arbitrary shape. There is no need to include boundary conditions explicitly. We see two major fields of application for the rotated staggered grid. The first is to realize numerical experiments in heterogeneous media with, for example, many empty cracks or voids. This can be used to validate rock properties and their effects on seismic wave propagation. The second field of application is modeling elastic waves in anisotropic media where, in contrast to standard staggered-grid schemes, no interpolation is necessary to calculate the Hooke summation. This can lead to a lower dispersion error and, since interpolation is quite CPU intensive, to a higher computational efficiency.

ACKNOWLEDGMENTS

E. H. S. thanks the Wave Inversion Technology (WIT) Consortium for their financial support. We thank M. Karrenbach for providing us with his displacement-stress FD code for further modifications. We also thank Assistant Editor G. T. Schuster, P. Moczo, and three anonymous reviewers for their helpful comments and suggestions. The simulations were performed at the Konrad-Zuse-Zentrum für Informationstechnik Berlin.

APPENDIX

DEFINATION OF MATRICES

As described in Igel et al. (1995), a convenient way to write the matrix $\hat{\mathbf{M}}$ is by introducing the matrices **A**, **B**, **C**, **D**, **E**, **F**:

$$\mathbf{A} = \begin{pmatrix} c_{11} & d_{\underset{12}{\rightarrow}} c_{16} & d_{\underset{13}{\rightarrow}} c_{15} \\ d_{\underset{12}{\leftarrow}} c_{16} & c_{66} & d_{\underset{13}{\rightarrow}} d_{\underset{12}{\leftarrow}} c_{65} \\ d_{\underset{13}{\leftarrow}} c_{15} & d_{\underset{12}{\rightarrow}} d_{\underset{13}{\leftarrow}} c_{65} & c_{55} \end{pmatrix}, \qquad \text{(A-1)}$$

$$\mathbf{B} = \begin{pmatrix} d^{\leftarrow}_{12}c_{16} & c_{12} & d^{\rightarrow}_{13}d^{\leftarrow}_{12}c_{56} \\ c_{66} & d^{\rightarrow}_{12}c_{62} & d^{\rightarrow}_{13}c_{52} \\ d^{\leftarrow}_{23}c_{14} & d^{\rightarrow}_{12}d^{\leftarrow}_{23}c_{64} & d^{\rightarrow}_{13}d^{\leftarrow}_{23}c_{54} \end{pmatrix}, \quad \text{(A-2)}$$

$$\mathbf{C} = \begin{pmatrix} d^{\leftarrow}_{13}c_{15} & d^{\rightarrow}_{12}d^{\leftarrow}_{13}c_{65} & c_{55} \\ d^{\leftarrow}_{23}c_{14} & d^{\rightarrow}_{12}d^{\leftarrow}_{23}c_{64} & d^{\rightarrow}_{13}d^{\leftarrow}_{23}c_{54} \\ c_{13} & d^{\rightarrow}_{12}c_{63} & d^{\rightarrow}_{13}c_{53} \end{pmatrix}, \quad \text{(A-3)}$$

$$\mathbf{D} = \begin{pmatrix} c_{66} & d^{\leftarrow}_{12}c_{62} & d^{\rightarrow}_{23}d^{\leftarrow}_{12}c_{64} \\ d^{\rightarrow}_{12}c_{62} & c_{22} & d^{\rightarrow}_{23}c_{24} \\ d^{\rightarrow}_{12}d^{\leftarrow}_{23}c_{64} & d^{\leftarrow}_{23}c_{24} & c_{44} \end{pmatrix}, \quad \text{(A-4)}$$

$$\mathbf{E} = \begin{pmatrix} d^{\rightarrow}_{12}d^{\leftarrow}_{13}c_{65} & d^{\leftarrow}_{13}c_{25} & d^{\rightarrow}_{23}d^{\leftarrow}_{13}c_{45} \\ d^{\rightarrow}_{12}d^{\leftarrow}_{23}c_{64} & d^{\leftarrow}_{23}c_{24} & c_{44} \\ d^{\rightarrow}_{12}c_{63} & c_{23} & d^{\rightarrow}_{23}c_{43} \end{pmatrix}, \quad \text{(A-5)}$$

$$\mathbf{F} = \begin{pmatrix} c_{55} & d^{\rightarrow}_{23}d^{\leftarrow}_{13}c_{54} & d^{\leftarrow}_{13}c_{53} \\ d^{\rightarrow}_{13}d^{\leftarrow}_{23}c_{54} & c_{44} & d^{\leftarrow}_{23}c_{43} \\ d^{\rightarrow}_{13}c_{53} & d^{\rightarrow}_{23}c_{43} & c_{33} \end{pmatrix}. \quad \text{(A-6)}$$

Then, using the above definitions, we can write

$$\hat{\mathbf{M}} = \frac{1}{\rho}\begin{pmatrix} \mathbf{kAk}^T & \mathbf{kBk}^T & \mathbf{kCk}^T \\ \mathbf{kBk}^T & \mathbf{kDk}^T & \mathbf{kEk}^T \\ \mathbf{kCk}^T & \mathbf{kEk}^T & \mathbf{kFk}^T \end{pmatrix}. \quad \text{(A-7)}$$

The elastic constants of the triclinic elastic medium (density $\rho = 1000\,\mathrm{kg/m^3}$) used for the comparison in Figure 2 are exactly the same as used in Igel et al. (1995). The factor 10^9 N/m^2 is omitted:

$$c_{tri} = \begin{pmatrix} 10 & 3.5 & 2.5 & -5 & 0.1 & 0.3 \\ 3.5 & 8 & 1.5 & 0.2 & -0.1 & -0.15 \\ 2.5 & 1.5 & 6 & 1 & 0.4 & 0.24 \\ -5 & 0.2 & 1 & 5 & 0.35 & 0.525 \\ 0.1 & -0.1 & 0.4 & 0.35 & 4 & -1 \\ 0.3 & -0.15 & 0.24 & 0.525 & -1 & 3 \end{pmatrix}. \quad \text{(A-8)}$$

REFERENCES

Blanch, J. O., Robertsson, J. O. A., and Symes, W. W., 1995, Modeling of a constant Q: Methodology and algorithm for an efficient and optimally inexpensive viscoelastic technique: Geophysics, **60**, 176–184.

Bohlen, T., 2002, Parallel 3-D viscoelastic finite difference seismic modeling: Computers and Geoscience, **28**, 887–899.

Bohlen, T., and Saenger, E. H., 2003, 3-D Viscoelastic finite-difference modeling using the rotated staggered grid—Tests of accuracy: 65th Annual International Meeting, European Association of Geoscientists and Engineers, Extended Abstracts, C44.

Bohlen, T., Giese, R., Müller, C., and Landerer, F., 2003, Modeling of seismic waves around a tunnel with irregular wall: 65th Annual International Meeting, European Association of Geoscientists and Engineers, Extended Abstracts, P242.

Boore, D. M., 1970, Love waves in nonuniform wave guides: Finite difference calculations: Journal of Geophysical Research, **75**, 1512–1527.

Carcione, J. M., Herman, G. C., and ten Kroode, A. P. E., 2002, Seismic modeling: Geophysics, **67**, 1304–1325.

Carcione, J. M., Kosloff, D., and Kosloff, R., 1988, Viscoacoustic wave propagation simulation in the earth: Geophysics, **53**, 769–777.

Carcione, J. M., Kosloff, D., Behle, A., and Seriani, G., 1992, A spectral scheme for wave propagation simulation in 3-D elastic-anisotropic media: Geophysics, **57**, 1593–1607.

Crase, E., 1990, High-order (space and time) finite-difference modeling of the elastic wave equation: 60th Annual International Meeting, Society of Exploration Geophysicists, Expanded Abstracts, 987–991.

Graves, R. W., 1996, Simulating seismic wave propagation in 3D elastic media using staggered-grid finite differences: Bulletin of the Seismic Society of America, **86**, 1091–1106.

Hestholm, S., 2002, Composite memory variable velocity-stress viscoelastic modelling: Geophysical Journal International, **148**, 153–162.

Hestholm, S. O., and Ruud, B. O., 1998, 3-D finite-difference elastic wave modeling including surface topography: Geophysics, **63**, 613–622.

Holberg, O., 1987, Computational aspects of the choice of operator and sampling interval for numerical differentiation in large-scale simulation of wave phenomena: Geophysical Prospecting, **35**, 629–655.

Igel, H., Mora, P., and Riollet, B., 1995, Anisotropic wave propagation through finite-difference grids: Geophysics, **60**, 1203–1216.

Karrenbach, M., 1995, Elastic tensor wavefields: Ph.D. thesis, Stanford University.

Kelly, K. R., Ward, R. W., Treitel, S., and Alford, R. M., 1976, Synthetic seismograms: A finite-difference approach: Geophysics, **41**, 2–27.

Komatitsch, D., Barnes, C., and Tromp, J., 2000, Simulation of anisotropic wave propogation based upon a spectral element method: Geophysics, **65**, 1251–1260.

Krüger, O. S., Saenger, E. H., and Shapiro, S., 2002, Simulation of the diffraction by single cracks: An accuracy study: 72nd Annual International Meeting, Society of Exploration Geophysicists, Expanded Abstracts, 2007–2010.

Levander, A. R., 1988, Fourth-order finite-difference P-SV seismograms: Geophysics, **53**, 1425–1436.

Luo, Y., and Schuster, G., 1990, Parsimonious staggered grid finite-differencing of the wave equation: Geophysical Research Letters, **17**, 155–158.

Marfurt, K. J., 1984, Accuracy of finite-difference and finite-element modeling of the scalar and elastic wave equations: Geophysics, **49**, 533–549.

Moczo, P., Kristek, J., and Halada, L., 2000, 3D 4th-order staggered-grid finite-difference schemes: Stability and grid dispersion: Bulletin of the Seismic Society of America, **90**, 587–603.

Moczo, P., Kristek, J., Vavrycuk, V., Archuleta, R. J., and Halada, L., 2002, 3D heterogeneous staggered-grid finite-difference modeling of seismic motion with volume harmonic and arithmetic averaging of elastic moduli and densities: Bulletin of the Seismic Society of America, **92**, 3042–3066.

Müller, T. M., and Shapiro, S. A., 2001, Most probable seismic pulses in single realizations of two- and three-dimensional random media: Geophysical Journal International, **144**, 83–95.

Müller, T. M., Shapiro, S. A., and Sick, C. M. A., 2002, Most probable ballistic waves in random media: A weak-fluctuation approximation and numerical results: Waves in Random Media, **12**, 223–245.

Ohminato, T., and Chouet, B., 1997, A free surface boundary condition for including 3D topography in the finite difference method: Bulletin of the Seismic Society of America, **87**, 494–515.

Oprsal, I., and Zahradnik, J., 1999, Elastic finite-difference method for irregular grids: Geophysics, **64**, 240–250.

Robertsson, J. O. A., 1996, A numerical free-surface condition for elastic/viscoelastic finite-difference modeling in the presence of topography: Geophysics, **61**, 1921–1934.

Robertsson, J. O. A., Blanch, J. O., and Symes, W. W., 1994, Viscoelastic finite difference modeling: Geophysics, **59**, 1444–1456.

Saenger, E. H., and Shapiro, S. A., 2002, Effective velocities in fractured media: A numerical study using the rotated staggered finite-difference grid: Geophysical Prospecting, **50**, 183–194.

Saenger, E. H., Gold, N., and Shapiro, S. A., 2000, Modeling the propagation of elastic waves using a modified finite-difference grid: Wave Motion, **31**, 77–92.

Saenger, E. H., Krüger, O. S., and Shapiro, S., 2002, Simulation of effective elastic properties of 3D fractured medium: 72nd Annual International Meeting, Society of Exploration Geophysicists, Expanded Abstracts, 1825–1828.

———2003, Numerical rock physics: The Gassmann equation: 73rd Annual International Meeting, Society of Exploration Geophysicists, Expanded Abstracts, 1278–1281.
Sei, A., 1995, A family of numerical schemes for the computation of elastic waves: SIAM Journal of Scientific Computing, **16**, 898–916.
Virieux, J., 1986, Velocity-stress finite-difference method: Geophysics, **51**, 889–901.
Xu, H., Day, S. M., and Minster, J.-B. H., 1999, Two-dimensional linear and nonlinear wave propagation in a half space: Bulletin of the Seismic Society of America, **89**, 903–917.
Zahradnik, J., and Hron, F., 1992, Robust finite-difference scheme fore elastic waves on coarse grids: Studia Geoph. Geod., **36**, 1–19.